A Deeper Look into REM Sleep: A Comparative Analysis of Methods

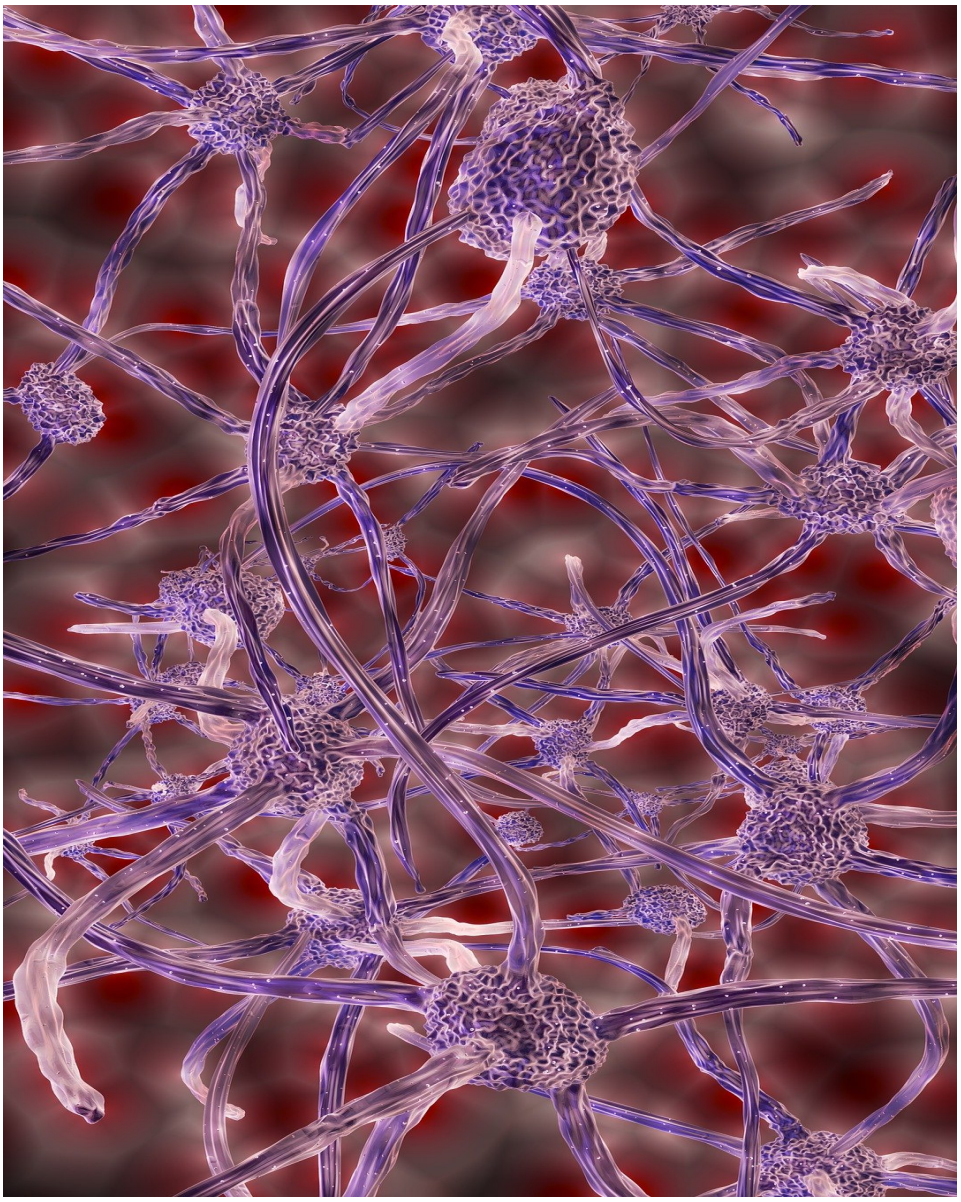

Denise N.A. Monkau

Layout: typeset by the author using LaTeX.
Cover illustration: Abstract Neurons Connection Blender 3D by MasterTux (Pixaday)

A Deeper Look into REM Sleep: A Comparative Analysis of Methods

Denise N.A. Monkau
12520519

Bachelor thesis
Credits: 18 EC

Bachelor *Kunstmatige Intelligentie*

University of Amsterdam
Faculty of Science
Science Park 904
1098 XH Amsterdam

Supervisor
Dr. A.N. (Abdelrahman) Rayan
Genzel Lab, Donders Institute

Dhr. Drs. T.R. (Taco) Walstra
FNWI, Univerisity of Amsterdam

March 22, 2025

Acknowledgements

I would like to acknowledge and thank my supervisors, Abdelrahman Rayan and Taco Walstra.

Firstly, my gratitude goes to Abdelrahman Rayan for positively and excitedly guiding me along with this project, always being open and opening up the world of research in Neuroscience for me in an incredibly welcoming manner. No lesser, Taco Walstra helped push my ideas and general approach into a personally fulfilling and Artificial Intelligence-oriented project while also guiding me along the more mathematical sides with quick responses and videos. Next, I wholeheartedly acknowledge Lisa Genzel for allowing me to start this project in the first place and finding time to give feedback. Lastly, I thank everyone at Genzel Lab involved with this project, the sleep scorers, other members and students who helped inspire this thesis.

Abstract

Theta and Gamma frequencies have a commonly known interaction; the methods in this thesis help with the analysis of this phenomenon. The data is brain waves during REM sleep from rats who participated in the Object Space Task under different conditions. This thesis presents three core methods: correlational (Cross Frequency Coupling) analysis, K-Means, and Hidden Markov Models. The first method finds the strong and weaker relationships between Theta and Gamma in the data. K-Means and Hidden Markov Models separate the Gamma bands over the Theta phase. These clusters are analysed to examine how well the methods can distinguish between frequency sets in a complex Theta phase range. The results show a significant distinction between lower and higher frequency bands, which is dependent on the correlational strength present in the data. The last two methods divided the Gamma bands across the Theta phase similarly. All methods' results led to converging outcomes. This alignment creates a cohesive statement that correlation and clustering methods can find meaningful Gamma clusters in an individual Theta cycle, thus, enabling analysis of Theta-Gamma coupling.

Keywords: *Amplitude, Brain, Clustering, Comodulation, Correlation, Coupling, Cross Frequency Coupling, Frequency, Hidden Markov Models, Hippocampus, K-Means, Oscillations, Phase, Prelimbic Prefrontal Cortex, Rat, Spectral Analysis, Statistics, Unsupervised Learning*

Contents

Glossary

Amplitude the strength of a signal in power.

Comodulation the occurrence of joint changes between signals.

Coupling the interaction between signals.

Frequency the number with which a signal crosses the time axis.

Oscillations the repetitive electrical activity from neural tissue.

Phase the position of a point in time on a waveform cycle.

Chapter 1

Introduction

Rapid Eye Movement (REM) sleep is commonly viewed as a complex and mysterious sleep state and is often associated with dreams connected to daily activities. The replay of these daily memories is known to strengthen them, which can have positive or negative effects as studied in scientific fields such as Psychology. In the study of the brain, behaviour, and cognition (Neuroscience), REM sleep and memory are analysed on various scales and linked together. The inter-connectivity of memories, sleep and general communication in the brain during sleep is the field of interest for this thesis.

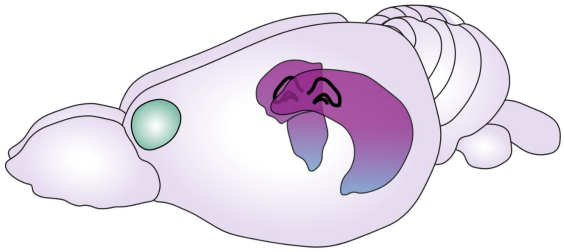

Figure 1.1: Schematic rat brain: the prefrontal cortex (left/green) and the hippocampus (right/purple) Klinzing et al. (2019)

While on the subject of memories, the hippocampus (HPC) and prefrontal cortex (PFC) are substantively involved (figure 1.1). The hippocampus is a seahorse-like area in both brain hemispheres and is placed deep in the temporal lobe (a brain region on the sides of the head). It is known as a "super hub" due to the region's high connectivity with other areas in the brain.
The prefrontal cortex is the area at the forefront of the brain, stomach side or 'dorsal'. Although the PFC is commonly known for its involvement in executive function, which is categorised as processes like planning, reasoning and decision making, it is a deeply layered (laminar) region with various responsibilities. One of which is memory regulation in collaboration with the hippocampus (figure 1.3).

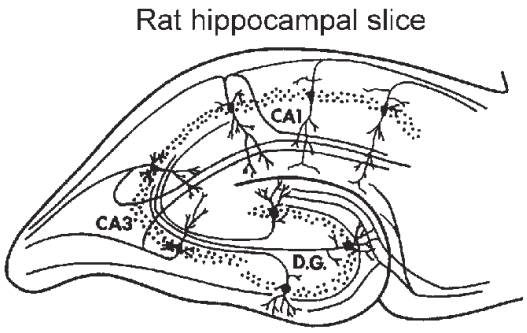

(a) Schematic diagram of rat Hippocampus showing respective areas Abbreviations CA1 area Szewczyk et al. (2001)

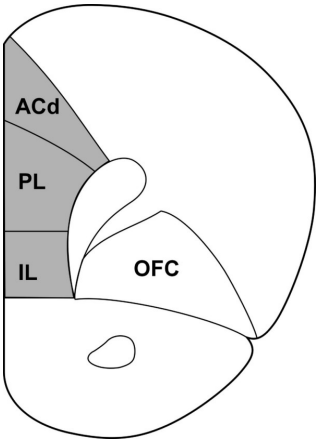

(b) A frontal segmentation of the rat brain showing the mPFC (shaded area) Michelsen et al. (2007)

Communication between the HPC and PFC happens through a multitude of factors such as the strength of a signal (amplitude), the occurrence of the waves along the time axis (phase), and the amount the signal crosses the time axis (frequency) in the brain waves (figure 3.2b & 3.2c). This thesis will look at all of these factors with frequency as its focal point; the interactions between frequencies influence the communication in the brain, mainly during sleep and memory processes (section 2.2).

In this thesis, Theta-Gamma coupling will be viewed with under-explored data, mainly with brain waves acquired from REM sleep. Through machine learning and statistics, I aim to find a significant and useful foundation to analyse the interactions between Theta and Gamma frequencies in the hippocampus and prelimbic cortex during REM sleep.

Correlational significance between (Theta and Gamma) filtered data bands is used to prove the interaction between the Theta and Gamma frequencies.

Three unsupervised machine learning techniques are applied to the data to establish clusters within the signal from the CA1 in the HPC (figure 1.2a) and the prelimbic prefrontal cortex (PrL-PFC) (figure 1.2b). I will interchangeably refer to these specific regions with HPC and PFC, respectively. Firstly, Community Detection is applied to retrieve the estimated cluster amount necessary for K-Means. The latter is an easily implementable and commonly used clustering technique. The K-Means model fits and predicts clusters within the data; these methods follow Zhang et al.. Our addition is a new strategy, Hidden Markov Model (HMM) clustering. I chose this due to its general use within Neuroscience research and its more nuanced probabilistic nature, perhaps creating better results Koski (1996), Florian et al. (2011). All the resulting clusters should be identifiable with a Gamma band. These Theta-Gamma clusters are each statistically assessed within themselves and in comparison to the other.

From these paragraphs, the question arises: can correlation and clustering methods

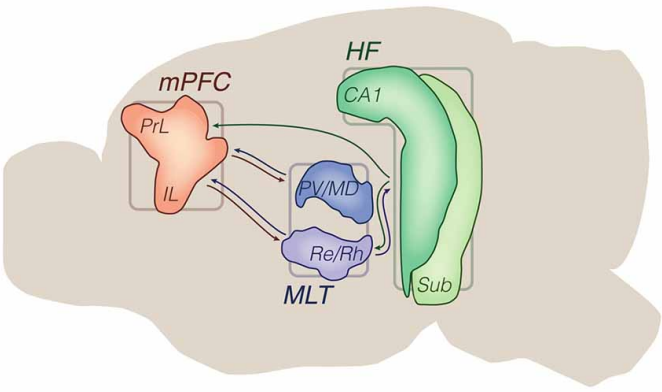

Figure 1.3: Schematic drawing of the CA1 of the hippocampus (HF) connection to the prelimbic (PrL) PFC Bueno-Junior & Leite (2018)

be used to examine Theta-Gamma coupling within the CA1 and PrL-PFC during REM sleep in rats?

The correlational approach should align with the other methods and former research for a positive outcome, meaning a significant correlation should yield a significant cluster. The clustering methods will be assessed through cluster quality and comparison. In this report, I explain the necessary background information within Neuroscience to contextualise this thesis. After which, the methods utilised for the observed results are described. The first approach assesses the correlations between Theta and Gamma frequencies in the data according to Kramer & Eden. Then, the Community Detection explains how the number of clusters is derived as stated by Zhang et al.. After which, the K-Means clustering with Pearson distance inspired by the same study and a new approach with Hidden Markov Models illustrate the means to find the Theta-Gamma clusters. The successive sections will present the former methods' results and a model evaluation based on the resulting clusters from both unsupervised learning methods.

Ultimately, I infer a conclusion on the correctness of using the mentioned Artificial Intelligence methods, unsupervised learning and statistical measures, through the alignment of the approaches mentioned and their respective statistics.

Chapter 2

Related Work

2.1 Theta-Gamma Coupling

This thesis focuses specifically on comodulation between the Theta-Gamma (TG) frequencies. This paragraph will give more background on the analysed frequencies and their use. Coupling is the interaction between oscillations, repetitive movements in the brain wave, at different frequency bands. Comodulation is the correlated fluctuation between the frequency waves. When one speaks about Theta-Gamma coupling, this encompasses the interaction between frequencies as a broad concept. In contrast, comodulation has established this interaction and works as a label.

The frequencies for this thesis have been studied and estimated at different numerical ranges. Theta oscillations have a frequency between 4 and 12 Hz. Gamma oscillations comodulate with Theta and divide into numerous subbands; they range in frequency from 20 to 150Hz. Following previous studies, I expect roughly three subbands within this frequency range Zhang et al. (2019).

Slow Gamma (20–50 Hz), which is dominant in stratum radiatum (SR), is associated with input from the CA3 sub-region of the hippocampus (HPC) (figure 2.1b). This oscillation plays a role in memory retrieval.

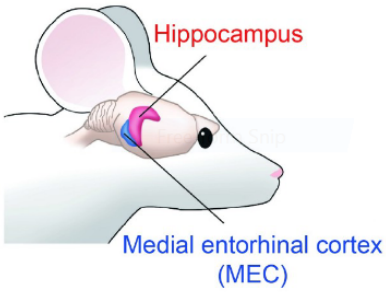

(a) hippocampus and medial enthorhinal cortex, containing the layer III of the Enthorhinal cortex in a rodent

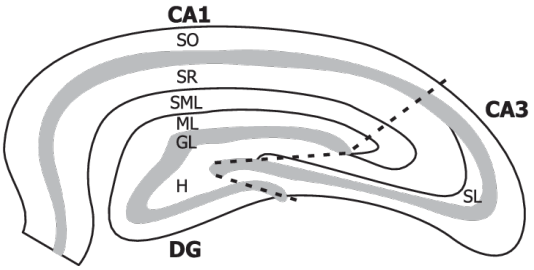

(b) Diagram of hippocampus in a rat with CA1, CA3, stratum radiatum (SR), stratum lacunosum-moleculare (SML),

Medium Gamma (40–120 Hz), most active in stratum lacunosum-moleculare (SML), takes input from layer III of the entorhinal cortex (EC) in the temporal lobe and is thought to encode ongoing sensory information (figure 2.1a).

Fast Gamma (120 Hz) is thought to represent local neural activity in specific areas of the CA1, stratum pyramidal cells.

Zhang et al. state time-wise organisation of these oscillations is poorly understood because current analysis methods obscure moment-to-moment change in Theta-Gamma coupling. Prior work has hypothesised that CA1 rapidly shifts between inputs from CA3, which are thought to be influential for memory retrieval, and inputs from EC to process ongoing sensory experiences. *'Rapid changes in Theta-Gamma coupling states from one Theta-cycle to the next coupled with the distinct coherence and neural coding of different TG states shows that the HPC rapidly shifts between distinct functional states'* Zhang et al. (2019). The Theta cycle in our results ranges from $-\pi$ to π in radians. So, the ascending phase is around $-\pi$ to zero, the peak at approximately zero, and the descending phase between zero and π. The slow Gamma state in awake and REM periods is dominant in 30-50 Hz and most prevalent in the descending phase of Theta Colgin et al. (2009). Furthermore, increased CA3-CA1 coupling was found during slow Gamma Colgin et al. (2009), Zhang et al. (2019), Lasztóczi & Klausberger (2016). Succeedingly, medium Gamma was found to be dominant in a 40-120 Hz range in the peak of Theta. Higher EC-CA1 coupling was discovered in the medium Gamma states than in the other three states (Slow Gamma, Early Fast Gamma and Late Fast Gamma) at 60-80 Hz during awake periods and 40-70 Hz during REM periods Zhang et al. (2019), Colgin et al. (2009), Amemiya & Redish (2018). Finally, fast Gamma occurred above 120 Hz at different phases of Theta; EF-Gamma was more present at the beginning of the ascending Theta phase and LF-Gamma was found around the end of the descending phase Zhang et al. (2019). This high Gamma band is excluded from the clustering methods due to its complexity and other frequency inferences. Furthermore, all the clustering results would be influenced if this Gamma was included.

In this thesis, oscillations from the CA1 and prelimbic PFC are utilised. So, it is expected to get a range for the Gamma subbands similar to former research, at least for the hippocampal CA1. Specifically, most research has found concise Theta-Gamma coupling in the HPC, not necessarily in the prelimbic PFC. Theta-Gamma coupling in the PFC is yet to be fully explored, making it an intriguing aspect of this thesis.

2.2 Memory, Hippocampus and Prefrontal Cortex

Memory is the storage of information in the brain; there are many different sub-classes of memory. An example is declarative memory, which encompasses explicit memories (e.g. dates, names, facts and events). In this thesis, the topic will intrinsically be on two main memory processes, memory consolidation and memory encoding. Memory consolidation is more prevalent during sleep than in a wake state. And memory encoding since this is more prevalent in REM sleep than nonREM (NREM) Genzel et al. (2015), Genzel & Wixted (2017), Schall & Dickson (2010). Memory consolidation is the process of sta-

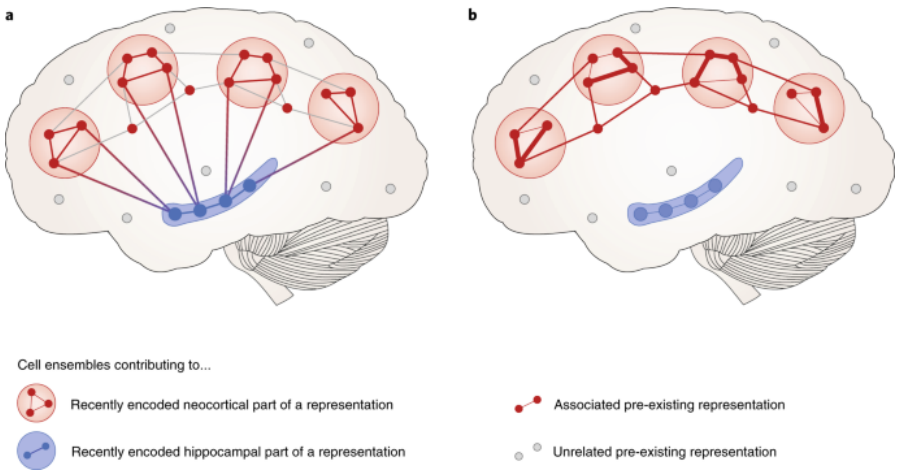

Figure 2.2: Schematic representation of system consolidation Klinzing et al. (2019)

bilising stored memories, which divides into cellular/synaptic and systems consolidation Genzel & Wixted (2017). Cellular consolidation is thought to be an "after-effect" of Long Term Potentiation (LTP), a prolonged and high rise in depolarisation of the synapses. In other words, this increases neuronal activity for a longer time. In contrast, systems consolidation works on a larger scale through the interplay between the hippocampus and PFC, which leads short-term memories dependent on the hippocampus to become more stable and independent of this brain region (figure 2.2). Another memory consolidation process is reconsolidation, similar to the reverse of systems consolidation, since it leads to re-malleability of memories, destabilising and making them available to alterations Squire et al. (2015). Memory encoding is the process by which sensory information translates to a data format accessible to other brain activities. There are many encoding types for different memories (e.g. visual, semantic and acoustic). The hippocampus and the PFC are regions that play an active part in the mentioned memory processes. Memory is not stored in one place in the brain but distributed across brain regions and partially connected. There are well-connected hubs in the brain, "superhubs", which are regions that hold or relay information from a lot of other brain regions; the hippocampus is one of these "superhubs" Genzel (2020). For example, the hippocampus holds a frequency concept called the Sharp Wave Ripple complex (SWR). These SWRs are high bursts of excitation in the CA3, which contains a lot of excitatory neurons connected to the rest of the hippocampus, leading to a positive feedback loop Squire et al. (2015). After this excitation/depolarisation through the hippocampus, the CA1 creates an offset in the local field potential (LFP), a summed electrical mass outside of the cell, which leads to another frequency pattern, ripples (150-200 Hz) Squire et al. (2015). Due to its many differences in and relationships between patterns, SWR carries different kinds of information and plays a significant role in memory consolidation Squire et al. (2015). This concept illustrates the established influences of frequency comodulation and memory in the hippocampus.

2.3 Memory during REM sleep

In this thesis, REM sleep is centralised with an intriguing background due to its similarity to the wake state. SWR plays a confounding role in memory consolidation and acts differently in sleep than in the wake state (section 2.2). Memory reactivation or reconsolidation is also expressed differently in these states. Hippocampal neurons that are active during simple track tasks induce reactivation when rewards are involved by cell stabilisation. This reaction also increases the likelihood of reconsolidation/reactivation later. Memory reactivation in REM sleep is more similar to wake than in NREM sleep state. The Theta frequency in the hippocampus influences REM sleep reactivation. *'Neurons active in familiar experiences were active again in the Theta trough in REM sleep, while neurons from novel experiences were active in the Theta peak'* Samanta et al. (2020). However, much is still unknown about reactivation during REM for rats Amemiya & Redish (2018). In the Theta trough, the minimum point in the cycle, neurons related to familiar experiences were activated in REM sleep Poe et al. (2000). The Theta frequencies have a known influence on memory processes that have a very different expression in REM sleep than in NREM. This difference could express itself in the results.

Chapter 3

Method

3.1 Data and Pre-processing

3.1.1 Data acquisition & Object Space Task

The data is acquired from the Object Space Task Genzel et al. (2019). This experiment focuses on declarative memory; rats walk through a square arena with objects (figure 3.1). These animals are conditioned on a stable state in which objects are fixed in place across all trials. In the test trial, one object's location changes. In the overlapping condition, one location remains constant across all sample trials and the second location changes. The locations in the last sample trial and test trial are the same. Finally, in the random state, the objects were pseudo-randomly, *'controlled for the equal appearance of all locations'* Genzel et al. (2019), changed. One dataset is from a condition where the rats had not left the home cage to perform the task, giving a baseline for the animals.

After the Object Space Task is performed by the rats, data is acquired from the CA1 in the HPC and the prelimbic PFC with a modified light custom-built microdrive during sleep. A microdrive is a small device with which neural signals are retrieved. It contains movable tetrodes implanted on the animal's head. Screws are fixed to the skull of the rats to stabilise this implanted structure. The screws and microdrive are placed with

Figure 3.1: Genzel Lab's Object Space Task

quick adhesive cement and dental acrylic cement. The cortical surface is covered in a sterile vaseline. Four of the rats have an over-expressive RGS14 gene: rats three, four, seven, and eight. The others are used for control, which could influence the results.

3.1.2 Data format

Matlab files were provided, containing tetrode readings from the rats' CA1 and prelimbic cortices during sleep and after the Object Space Task (section 3.1.1). These readings have a sample rate of 1000 milliseconds and are measured in μV, where V is Voltage.

Furthermore, I obtained an array of sleep scores, ranging from one to five, where five is REM sleep. The sleep scoring was done by Anumita Samanta and Eva Severijnen of Genzel Lab. These sleep scores facilitate filtering REM sleep periods out of the raw data. The scores aligned with the sample rate; one score covered a 1000 millisecond section of data.

All source code used in this thesis is available in the GitHub repository `https://github.com/DnaMonkau/Theta_Gamma_Clustering`.

3.1.3 Spectral Analysis

Firstly, I perform a spectral analysis on the REM data acquired to visualise the frequency distribution in the data (section 3.1.2).
The Discrete Fourier Transform (DFT) retrieves an estimate of the power spectral density (PSD), describing the frequency distribution. I use P. Welch's method for DFT to extract the final result Welch (1967); this approaches the transform through overlapping batches, which gives smoother frequency power representations, making it easier to analyse.

Discrete Fourier Transform

As the name of this transform suggests, the Discrete Fourier Transform is applied to a discrete sample of a signal. The Fourier Transform is utilised in this sample, which uses weights to transform complex numbers dependent on time in seconds (signals) to numbers dependent on frequency in Hertz (Hz), where the frequency is defined by equation 3.1. The standard Fourier transform assumes a continuous signal (equation 3.2).

$$Frequency(Hz) = \frac{1}{seconds(s)} \tag{3.1}$$

$$F(k) = \int_{-\infty}^{\infty} f(t)e^{-jkt}dt \tag{3.2}$$

$$e^{-j\omega n} = \cos(\omega n) - j\sin(\omega n) \tag{3.3}$$

However, when the number n of signals is known, the function is discretised to the Discrete Fourier Transform (equation 3.4), where a specific sample N is taken of the continuous signal and k gives the frequency. Euler's formula (equation 3.3) gives the

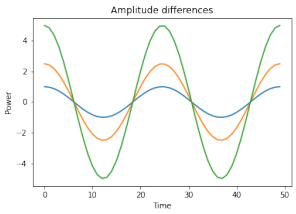

(a) Example of amplitude shifts in a sinusoid

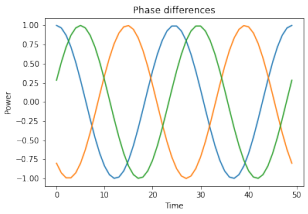

(b) Example of phase shifts in a sinusoid

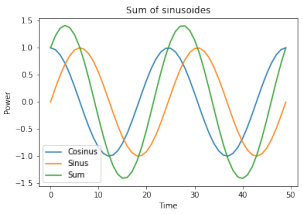

(c) Example of the sum of sines and cosines

means to put the previous estimation following a repeating (periodic) range (equation 3.5), where the signal is distributed alongside a sum of cosines and sinuses (figure 3.2c).

$$\sum_{n=0}^{N} f(n) e^{\frac{-2\pi j(k-1)(n-1)}{N}} \tag{3.4}$$

$$\begin{aligned} e^{\frac{-2\pi(k-1)(n-1)}{N}} &= cos(\frac{2\pi(k-1)(n-1)}{N}) + j\sin(\frac{2\pi(k-1)(n-1)}{N}) \\ F(k) &= \sum_{n=0}^{N-1} f(n) e^{\frac{-2\pi(k-1)(n-1)}{N}} \end{aligned} \tag{3.5}$$

Power Spectrum

The PSD is retrieved with the Discrete Fourier Transform. The summation of each weighted signal leads to positive and negative effects on the signal. This process shows clear positive power density peaks in the data per frequency, represented by equation 3.6, where δ is 1000, T is the total time of the recording, and $F(k)^*$ is the complex conjugate of the DFT. This spectral result could also be viewed logarithmically, giving a more general overview (equation 3.7). Subsequently, this expresses the power of each frequency in Decibels (dB) along a negative axis in our data, where more positive values represent a relatively more involved frequency in the REM data.

$$\begin{aligned} f &= \frac{2\Delta^2}{T} F(k) F(k)^* \\ S &= |f^2| \end{aligned} \tag{3.6}$$

$$S = \frac{10}{max|f^2|} \log_{10} |f^2| \tag{3.7}$$

Welch's Method

Additionally, Welch applies a step before the Discrete Fourier Transform. Initially, this method splits the data into segments with 50% overlapping data (figure 3.3). Collaboratively, the data is sampled every 2.0 Hz. Lastly, a "Hamming" window fits onto the data.

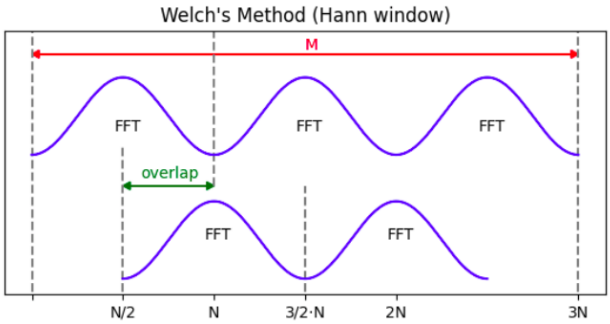

Figure 3.3: P. Welch's method illustrated through overlapping segments with Hanning window (a less extensive version of Hamming) Martinez et al. (2021)

I tested multiple numbers for the amount of segments Welch should take, ranging from 25 to 125 with steps of 25, and 100 segments is the most distinguished approximation based on the smoothing and information retained within the plots. The other parameter, a sampling frequency of 2.0 Hz, was suggested by our supervisor based on his experience with the data. The other factors were defaults within the function used.
The results from the former paragraph give a clearer view of the frequency distribution in the data, which is important to understand for the Cross Frequency Coupling and further clustering.

3.2 Cross Frequency Coupling

This thesis' Cross Frequency Coupling or Phase-Amplitude Coupling (PAC) follows the method by Kramer & Eden. Starting with the Spectral Analysis (section 3.1.3). Next, the data is filtered into lower and higher frequency bands with pre-estimated bands. Afterwards, the amplitude and phase are extracted from this filtered data. Lastly, the significance of the relation between the amplitude and phase is determined Kramer & Eden (2020).

3.2.1 Filtering

As stated in section 3.2, the established frequency bounds from former research are utilised to filter the REM data the pre-estimated Theta (4-12 Hz), slow Gamma (25-59 Hz), medium Gamma (60-120), and fast Gamma (120-150 Hz) adopted by former research provide the filter Zhang et al. (2019), Schomburg et al. (2014). The Nyquist frequency is half the sample rate, 500 Hz. A Firwin function generates the coefficients with which the data is filtered for each frequency. This function takes the Nyquist frequency, the frequency's bounds and a Hamming window to cut off the coefficients (pseudocode A.1). Succeedingly, the coefficients are individually multiplied with data points and offset by weights in a clockwise followed by counter-clockwise manner, resulting in a filtered version

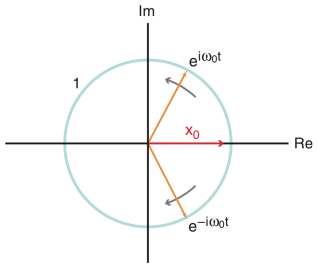

Figure 3.4: Signal illustrated along its real (Re) axis and cyclic axis (Im) Kramer & Eden (2020)

of the original data (equation 3.8). Appendix A.2 shows a sample of the resulting data.

$$\begin{aligned} y_i &= \sum_{k=1}^{M}\sum_{j=1}^{N}(x_{i-j} * b_k) - y_{i-j} \\ \hat{y}_i &= reverse(\sum_{k=1}^{M}\sum_{j=1}^{N}(reverse(y)_{i-j} * b_k) - \hat{y}_{i-j}) \end{aligned} \tag{3.8}$$

3.2.2 Amplitude and Phase

Ensuingly, the filtered data gives the means to extract the amplitude and phase through the Hilbert transform.

Hilbert Transform

The Hilbert transform gives a simplified version of the original signal and yields only positive frequencies (equation 3.9). Subsequently, the transformed data is added to the original data to give the analytic envelope, smooth mapping of the extrema in the data. Equation 3.10 illustrates this process, where k moves along the frequency axis, H is the Hilbert transform, $s(t)$ is the signal with positive and negative peaks, jx is the transformation of a signal part, and z is the analytic signal. The negative frequency aspects are transformed into positive ones through the Hilbert transform.

$$\begin{aligned} H[\hat{s}(t)] = H[x_0] &= \begin{cases} -jx & \text{if } k > 0 \\ 0 & \text{if } k = 0 \\ jx & \text{if } k < 0 \end{cases} \\ H[x_0] &= -je^{jkt} + je^{-jkt} \end{aligned} \tag{3.9}$$

$$\begin{aligned} y_0 &= H[\hat{s}(t)] \\ x_0 = s(t) &= e^{jkt} + e^{-jkt} \\ z_0 &= x_0 + iy_0 \end{aligned} \tag{3.10}$$

The amplitude within the Gamma frequency bound data is extracted through the absolute over the Hilbert transformed Gamma data; the amplitude represents the power(μV) of the Gamma data at each point.

The phase of the Theta frequency filtered data is determined by the angle over the Hilbert-transformed Theta data. This phase shows the instance of the Theta frequency occurring in time (milliseconds/ms).

Assessing these two factors is equal to determining the relationship between Theta waves occurring and the power in a Gamma subband along the time axis.

3.2.3 Cross-Frequency Coupling

Eventually, the significance values of the relation between the Theta phase and Gamma amplitudes are retrieved. I achieve this by rejecting the null hypothesis (H_0), which states that any variance in the results is not due to distinct differences but random or erroneous data sampling. I generate 1000 random surrogates for each difference between the minimum and maximum of the Gamma amplitude over the Theta phase is extracted and gives a set of h's. The same is done for the actual Gamma value, creating a singular true h for each surrogate set.

P value

The p value here intrinsically gives the probability of the random samples overlapping with the true value. Surrogates consisting of the randomly extracted Gamma amplitudes samples get compared to the complete Gamma observation. When there is a larger difference between the extrema of the averaged amplitude for a point in the Theta phase in the surrogates, it gets retained as significant. The p value results from the average of all retained surrogate's maximum distance between extrema in their amplitude, Hs_n (equation 3.11). The Theta phase should not be able to map higher and lower amplitude points in the random Gamma samples than in the true values. When there is comodulation, the Gamma amplitude should exceed the random ones. If the p value is small, the uniqueness of the true value increases.

$$\begin{aligned} p &= \frac{1}{N}\sum_{n=0}^{N} Hs_n \delta(Hs_n, h) \\ \delta(Hs_n, h) &= \begin{cases} 1 & \text{if } Hs_n > h \\ 0 & \text{otherwise} \end{cases} \end{aligned} \tag{3.11}$$

The p values represent the strength of the correlation between Theta and Gamma in our data, comodulation. A significant correlation is defined by p>0.05. Less correlated aspects of the data will likely yield poorer clusters, adding to the explanation of some clustering results.

3.3 Clustering

The Theta cycle is extracted by passing various features of Theta and the REM data to a Matlab script with which I retrieve a Frequency Phase Power (FPP) matrix `https://github.com/elifesciences-publications/IndividualThetaCluster/blob/master/Demo_SingleThetaCluster.m` Zhang et al. (2019). Louvain's method is applied for Community Detection within the FPP matrix. The communities' subtotal is used as the k for K-Means, separated for regions, and averaged to spread across all rats. K-Means yields Theta-Gamma frequency clusters. Besides this method, Hidden Markov Models are applied to the FPP matrix to cluster the REM sleep data where the hidden variable becomes the most optimal Gamma division.

As mentioned in section 2.1, the fast Gamma is excluded from these methods due to its complexity. This choice avoids baseless assumptions about the fast Gamma in the data. Furthermore, my supervisors and I believe the other frequency bands can yield enough results to assess the clustering methods.

3.3.1 Frequency Phase Power Matrix

Before clustering, the data needs to be reshaped into frequency phase power matrices. This matrix re-instantiates the data into power vectors of shape 1020 (frequency×phase), intrinsically yielding individual Theta cycles in terms of phase with Gamma power and frequencies. The 51 frequencies span across 20-120 Hz with intervals of two. Furthermore, the phase divides into 20 bins; an individual Theta cycle corresponds to the identifiable repeating wave in the data from $-\pi$ to π (360 degrees. Lastly, the power is in μV Zhang et al. (2019). The vectors sort into clusters to which one can assign Gamma band labels; once they get reshaped into a matrix of the shape number-of-vectors×frequency×phase. This data form gives images with a frequency and phase axis (figure 3.5). I use the power vectors of length 1020 in each cluster to pass through to the distance functions. The clustering quality is found by comparing distances between vectors (section 3.3.5).

3.3.2 Community Detection

I utilise the iterated Louvain method for Community Detection; This version of Louvain generates a more converged result than the non-iterated method. Louvain aims to optimise the overall modularity, Q, which measures the communities' quality by comparing the closeness of the linked data within the estimated cluster and across clusters. Equation 3.12 presents the formula for modularity, A represents the FPP-sampled adjacency

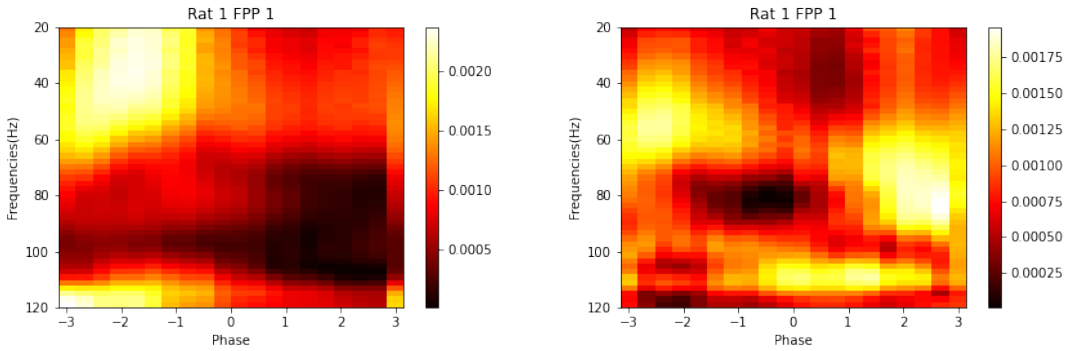

(a) The CA1 in the hippocampus

(b) The prelimbic prefrontal cortex

Figure 3.5: Frequency Phase Power Matrices from the PrL-PFC and CA1 in the home cage

matrix, N is the sum of all distance costs between nodes, k is the costs' sum for a vector's assigned community cluster, and c is the community to which the node belongs. Optimising Q leads to the most optimal community assignment.

$$Q = \frac{1}{2N}\sum_{ij}[A_{ij} - \frac{k_i k_j}{2N}]\delta(c_i, c_j)$$
$$\delta(c_i, c_j) = \begin{cases} 1 & if\ c_i = c_j \\ 0 & \text{otherwise} \end{cases} \tag{3.12}$$

The resulting communities are solely used for their total count as, it has been stated to not be an optimal clustering technique for this kind of data Zhang et al. (2019). The number of communities found indicate the amount of clusters which I expect in the following clustering methods.

3.3.3 K-Means Clustering

K-Means is applied to the FPP vectors (length = 1020) with a Pearson distance measurement function and K-Means++ for locating the centre/core points of the clusters, centroids. This algorithm is commonly used for clustering and is easily implementable. I apply K-Means from the *pyclustering* cluster package with a custom distance function as mentioned.

K-Means++ takes and optimises k centroids within the data. Then, it measures the distance of each data sample to these points. This variant of K-Means initialises sparsely distributed centre points; the first centroid is picked randomly, the rest of the data is compared to this centre point, and the point with the farthest distance is chosen to be the other centroid. This selection process is repeated until k centre points are found.

Following this initial step, the remaining points are assigned to their closest centroids and the cluster centres are recalculated based on the means of the draft clusters.

These steps are repeated until convergence is reached. Rule 3.13 describes the cluster assignment function, S_i; all x data points belong to the cluster when the distance to the centroid m of the cluster S_i is smaller than that to any other centroid. These centroids span over all clusters, making the optimal centroid and cluster easily determined for each FPP vector.

$$S_i^{(t)} = \{x_p : \|x_p - m_i^{(t)}\|^2 \leq \|x_p - m_j^{(t)}\|^2 \ \forall j, 1 \leq j \leq k\} \tag{3.13}$$

The data is fitted to this method and a prediction based on this is expelled, which results in a list containing k other lists with the indices for each power vector. Thus, each vector is assigned to a cluster.

3.3.4 Hidden Markov Model Clustering

A Gaussian Mixture Hidden Markov model is generated from the *hmmlearn* toolbox and fitted to the FPP vectors from which a prediction on the same data is extracted. The specific cluster number is passed through to the model by Community Detection (section 3.3.2). I choose to process the REM sleep data through FPP due to the HMM's connective nature and the cyclic Theta. It also keeps the thesis more self-contained and decreases variable factors for the model comparison.

Hidden Markov Modelling is an unsupervised learning method with which the data is given Bayesian probabilities on the likelihood of one state following another according to a specific set of model parameters. Hidden Markov Models are used for clustering as generative models, which use generated classes and calculate the likelihood of the data belonging to said class. In Hidden Markov Models, the unknown Gamma bands can be incorporated as hidden states or clusters. Figure 3.6 illustrates an example of state transitions with probabilities, a and b, in Hidden Markov Models.

The Hidden Markov modelling can be decomposed into three conceptual problems: the evaluation, decoding, and learning problems. Each problem confronts the actions of the HMM; the evaluation problem is central during the creation of the model, the learning problem is present in the model fitting, and the decoding problem is prevalent when specifying which sequence of hidden states is the optimal match with the data during the prediction of the clusters.

Evaluation problem

As mentioned, the evaluation problem is fundamental for the model's relation with the data (fitting). It intertwines with the decoding problem by having the same base but is centralised around the correctness of the model and its parameters than the hidden states. Equation C.1 in the appendix presents the mathematical aspects of the evaluation algorithm.

Learning problem

Collaboratively, solving the learning problem is finding the correct parameters for the model, which will be used in predicting the hidden sequences. The learning problem is

solved by gradient-based optimisation of the parameters in the model, retrieved from fitted data. The parameters get adjusted with steps derived from statistic measurements of the data until convergence is reached (equation C.2).

Decoding problem

Finally, the decoding problem is a matter of optimising the hidden sequences' quality. This problem occurs during the prediction of the clusters. Each FPP vector is run through the Viterbi algorithm and assigned to the hidden sequence with the highest likelihood of matching the visible states, segments of the set of FPP vectors before clustering. The number of communities found, k, yields the necessary number by which the HMM state map with FPP vectors is segmented. Hidden sequence estimation is a clustering method due to the equal test and training data. The most similar hidden states, FPP vectors, will align with each other based on the likelihood of tracing the observed partitions of the un-clustered vector segment. The optimisation algorithm retrieves the sample with the maximum probability amongst all possible cluster divisions based on the formerly mentioned transition, a, emission, b, and observation, v, probabilities (equation C.3). This algorithm results in a list of assignments for each vector with a label from a set containing k numbers.

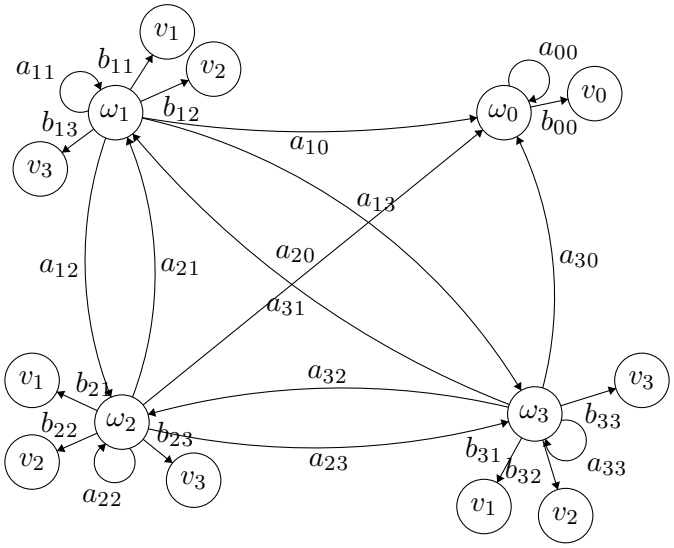

Figure 3.6: Schematic representation of Hidden Markov Model;

3.3.5 Cluster Significance

The K-Means and HMM quality is measured with inter-and intra-cluster results based on distance functions. These measurements were chosen based on their familiarity or lack of linear assumptions (appendix D). I apply the Pearson distance due to its involvement in former research Zhang et al. (2019). However, this function assumes that the relationships within the data are linear by assessing such a correlation among vectors. The Mahalanobis distance was chosen because it avoids this assumption by measuring the distance between a vector and the distribution of its cluster. This distance measurement searches for outliers rather than inliers. Inter-cluster significance views the difference between an item in a cluster and all the items outside of said group. A high number would indicate a stronger correlation of a vector to a cluster outside its own. In contrast, intra-cluster significance compares data inside the cluster, making a smaller intra-than inter-cluster distance a positive result. The results for each cluster are averaged giving their overall strength.

Model Comparison: Hidden Markov Model & K-Means

Lastly, I compare the intra-and inter-cluster Mahalanobis results from the HMM and K-Means clustering. The experiment conditions are merged to retrieve the complete model's mean and standard deviation for the Mahalanobis distances. Through this, the intra-and inter-cluster results are compared across models. I refrain from using Pearson since averaging is more complex within this distance measure.

T-test or Mann-Whitney could be applied to find the significance of model differences; the T-test assumes a normal distribution, a distribution with no out-of-place data points. Mann-Whitney is a non-parametric function. The former aims to disprove the null hypothesis by comparing two means. Meanwhile, the latter tests the H_0 by evaluating randomly drawn samples to one another. Mann-Whitney is used within this thesis due to results not being smoothly connected and the relatively small sample size of 54 points, three conditions containing 16 outcomes each and one with six results.

The averaged Mahalanobis results aid in comparing each clustering method per region. In addition, Mann-Whitney estimates the significance of the result differences across the two methods, which helps evaluate the similarity.

Chapter 4

Results

4.1 Spectral Analysis

The spectral analysis shows the distribution of the frequencies throughout the REM sleep data. I found similar results across rats and REM sleep periods, with a high peak around 8-12 Hz, a relatively lower one at 25-60Hz and a subtle yet notable rise around 100 Hz (figure 4.1). These results indicate a frequency band's involvement in the data and hold value when looking at the final results.

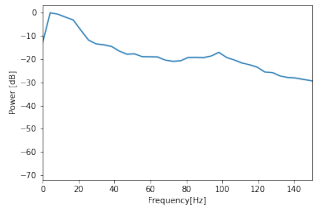

(a) Spectral Plot: Stable PFC Rat 1

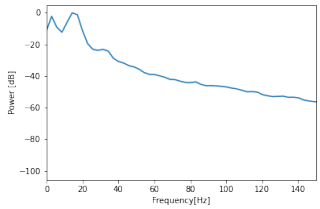

(b) Spectral Plot: home cage HPC Rat 1

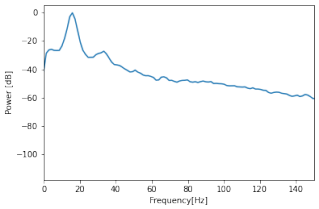

(c) Spectral Plot: Overlapping HPC Rat 3

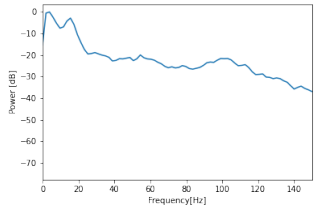

(d) Spectral Plot: Homecage PFC Rat 3

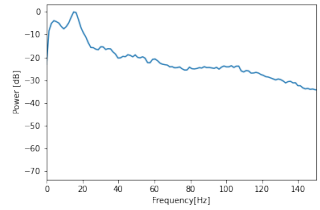

(e) Spectral Plot: random PFC Rat 7

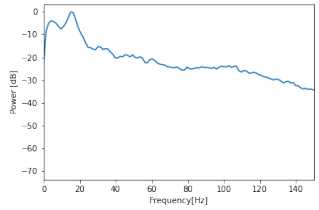

(f) Spectral Plot: overlapping PFC Rat 7

Figure 4.1: Spectral Plots with P. Welch processing from, in last REM sleep period of rat

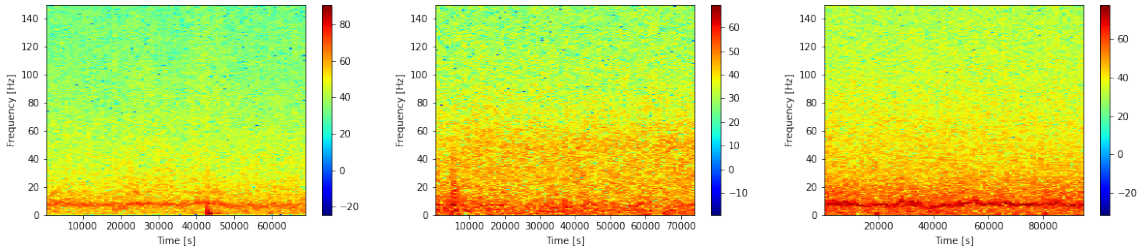

(a) Spectrogram: Rat 1 (b) Spectrogram: Rat 4 (c) Spectrogram: Rat 7

Figure 4.2: Spectrograms from PFC and HPC

4.2 Cross Frequency Coupling

The p values signify the correlational strengths between the Theta and Gamma frequencies in the data. Figure B.1 in appendix B gives a random sample out of all REM periods to visualise the method's results as described in section 3.2.3 and equation 3.11. The rats

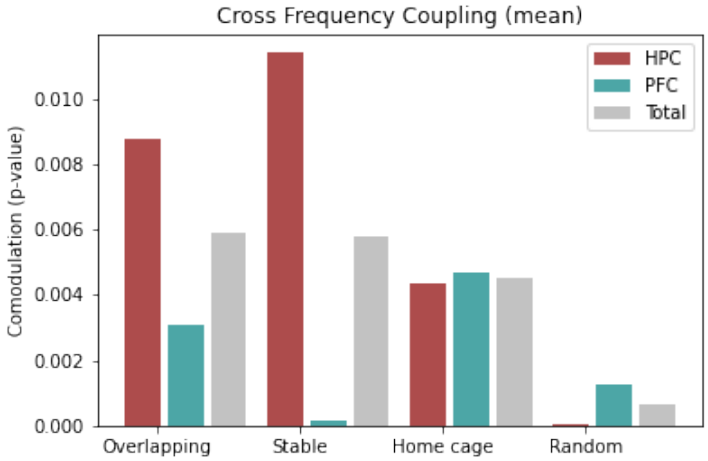

Figure 4.3: Average correlational results for each condition and region

yielded similar quality results in equivalent areas across conditions during REM sleep for the Theta-Gamma comodulations with an exception on the Stable condition data (table 4.3). Rats with a relatively poor comodulation in one condition also did in the others. In all conditions, the comodulation in Theta-slow Gamma correlation was significant ($p < 5.00\text{E-}02$) except for the PrL-PFC area in rat seven and CA1 area in rat nine for one condition each (table 4.2 & 4.4). Medium Gamma-Theta correlation has similar results; most rats have a strong comodulation. The only exception to this is in the hippocampal area of rat four for two conditions (table 4.4 & 4.2. Lastly, Theta to fast Gamma has a strong relationship through all conditions. However, these results do not completely re-

Rat	Over-Expression/Control	Region	Theta - slow Gamma	Theta - medium Gamma	Theta - fast Gamma
1	Control	HPC	4.00E-04	0.00E+00	0.00E+00
1	Control	PFC	2.62E-02	0.00E+00	1.00E-04
2	Control	HPC	0.00E+00	0.00E+00	0.00E+00
2	Over-Expression	PFC	2.27E-04	0.00E+00	1.82E-04
3	Over-Expression	HPC	0.00E+00	0.00E+00	0.00E+00
3	Over-Expression	PFC	0.00E+00	4.17E-05	4.17E-05
4	Over-Expression	HPC	2.78E-05	0.00E+00	0.00E+00
4	Over-Expression	PFC	2.22E-04	0.00E+00	2.78E-05
6	Control	HPC	0.00E+00	0.00E+00	0.00E+00
6	Control	PFC	0.00E+00	0.00E+00	0.00E+00
7	Over-Expression	HPC	0.00E+00	2.86E-04	5.71E-04
7	Over-Expression	PFC	0.00E+00	1.21E-03	7.14E-05
8	Over-Expression	HPC	1.36E-04	0.00E+00	0.00E+00
8	Over-Expression	PFC	0.00E+00	1.68E-03	0.00E+00
9	Control	HPC	0.00E+00	0.00E+00	0.00E+00
9	Control	PFC	0.00E+00	0.00E+00	0.00E+00

Table 4.1: Random condition, correlation results

Rat	Over-Expression/Control	Region	Theta - slow Gamma	Theta - medium Gamma	Theta - fast Gamma
1	Control	HPC	0.00E+00	6.25E-04	0.00E+00
1	Control	PFC	2.50E-04	6.25E-05	4.06E-03
2	Control	HPC	0.00E+00	1.76E-02	0.00E+00
2	Control	PFC	0.00E+00	4.58E-04	1.67E-04
3	Over-Expression	HPC	0.00E+00	0.00E+00	0.00E+00
3	Over-Expression	PFC	0.00E+00	0.00E+00	0.00E+00
4	Over-Expression	HPC	7.62E-04	8.22E-02	8.10E-04
4	Over-Expression	PFC	6.19E-04	3.10E-03	1.43E-04
6	Control	HPC	2.14E-03	0.00E+00	0.00E+00
6	Control	PFC	0.00E+00	0.00E+00	1.36E-04
7	Over-Expression	HPC	0.00E+00	0.00E+00	0.00E+00
7	Over-Expression	PFC	9.73E-02	5.00E-04	2.33E-03
8	Over-Expression	HPC	0.00E+00	0.00E+00	0.00E+00
8	Over-Expression	PFC	2.85E-03	0.00E+00	1.92E-04
9	Control	HPC	0.00E+00	0.00E+00	0.00E+00
9	Control	PFC	0.00E+00	0.00E+00	0.00E+00

Table 4.2: Home cage condition, correlation results

Rat	Over-Expression/Control	Region	Theta - slow Gamma	Theta - medium Gamma	Theta - fast Gamma
1	Control	HPC	3.26E-02	1.32E-02	3.00E-03
1	Control	PFC	1.07E-04	0.00E+00	2.86E-04
3	Over-Expression	HPC	1.15E-04	1.40E-02	5.58E-03
3	Over-Expression	PFC	0.00E+00	0.00E+00	5.38E-04

Table 4.3: Stable condition, correlation results

flect the true fast Gamma due to noise involvement and interference of other bands in the higher frequency data. Figure 4.3 shows the random condition has the most significant comodulation, followed by the home cage condition. The stable experiment condition has few results, but the comodulation across is significant in all REM periods present. Lastly, the overlapping dataset has the overall poorest comodulation. The same ranking remained after excluding fast Gamma. It is notable that in the two better performing conditions, HPC performs better than PFC. In the lesser conditions, the CA1 showed less significant results than the prelimbic prefrontal cortex. In general, the Cross Frequency

Rat	Over-Expression/Control	Region	Theta - slow Gamma	Theta - medium Gamma	Theta - fast Gamma
1	Control	HPC	0.00E+00	4.34E-02	0.00E+00
1	Control	PFC	8.13E-04	6.25E-05	8.75E-04
2	Control	HPC	0.00E+00	4.27E-03	0.00E+00
2	Control	PFC	0.00E+00	0.00E+00	4.55E-05
3	Over-Expression	HPC	0.00E+00	0.00E+00	0.00E+00
3	Over-Expression	PFC	7.14E-05	0.00E+00	0.00E+00
4	Over-Expression	HPC	1.37E-02	8.21E-02	2.94E-05
4	Over-Expression	PFC	8.53E-04	2.94E-05	5.88E-05
6	Control	HPC	5.08E-03	0.00E+00	0.00E+00
6	Control	PFC	0.00E+00	0.00E+00	8.33E-05
7	Over-Expression	HPC	0.00E+00	0.00E+00	0.00E+00
7	Over-Expression	PFC	1.32E-02	4.76E-02	6.00E-04
8	Over-Expression	HPC	0.00E+00	0.00E+00	0.00E+00
8	Over-Expression	PFC	4.38E-04	4.63E-035	0.00E+00
9	Control	HPC	6.20E-02	0.00E+00	0.00E+00
9	Control	PFC	4.15E-03	5.00E-05	0.00E+00

Table 4.4: Overlapping condition, correlation results

Coupling Analysis yielded significant comodulation, showing some coupling within our data between the Theta and Gamma bands.

4.3 FPP Clusters: K-Means

K-Means yielded significant results as expected from the spectral and CFC analysis. There were clear distinctions between clusters in the hippocampus; one often being in a frequency range of 20-80 Hz with a centre around 40 Hz in the ascending Theta phase and the other in a range of 80-120 Hz with a centre around 100 Hz around the peak and descending phase. The division of clusters in the prelimbic prefrontal cortex was slightly less cohesive with a range of 20-80/100 Hz and 80/100-120 Hz centred around 40 or 80/110 Hz, respectively (figure 4.4). The lowest frequency peaked in power around the ascending phase and the higher values were more present around the peak.

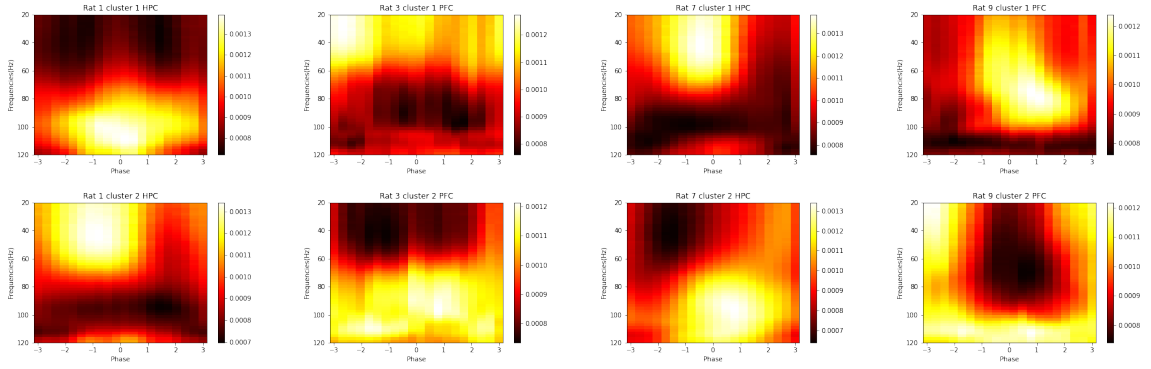

Figure 4.4: K-Means of rat one (HPC, random and control), three (PFC, random and over-expression), seven (HPC, overlapping and over-expression) and nine (PFC, random and control)

4.3.1 Significance: Intra-cluster & Inter-cluster

Each cluster's intra-and inter-distance was measured. The former indicates the cluster strength, while the latter shows the lack of coherence within the cluster. All of the distance function results are attainable under `https://github.com/DnaMonkau/Theta_Gamma_Clustering`. The Mahalanobis and Pearson distance of the cluster sets are presented in table 4.5 and 4.6 for the HPC and PFC. A smaller intra-than inter-cluster distance is preferable as this shows the cluster's internal relations are more significant than external. The Pearson intra-cluster distances were estimated at around 50% less than inter-cluster. For Mahalanobis, a smaller difference and sometimes an unfavourable result, the inter-cluster significance being lower than or equal to the intra-cluster distances, were noted. However, the general Mahalanobis results were affirming; they presented a lower intra-cluster than inter-cluster distance.

Rat	Cluster Number	Region	Over-Expression/Control	Condition	Pearson Distance Inter	Pearson Distance Intra
1	1	HPC	Control	Random	6.28E-01	3.23E-01
1	2	HPC	Control	Random	6.30E-01	3.23E-01
3	1	PFC	Over-Expression	Random	6.14E-01	3.44E-01
3	2	PFC	Over-Expression	Random	6.05E-01	3.62E-01
7	1	HPC	Over-Expression	Random	6.17E-01	3.29E-01
7	2	HPC	Over-Expression	Overlapping	6.15E-01	3.32E-01
9	1	PFC	Control	Overlapping	6.31E-01	3.09E-01
9	2	PFC	Control	Random	6.04E-01	3.51E-01

Table 4.5: K-Means: intra-and inter-cluster Mahalanobis distances for rat one (HPC and control), three (PFC and over-expression), seven (HPC and over-expression) and nine (PFC and control)

Rat	Cluster_Number	Region	Over-Expression/Control	Condition	Mahalanobis Distance Inter	Mahalanobis Distance Intra
1	1	HPC	Control	Random	1.66E+01	1.38E+01
1	2	HPC	Control	Random	1.67E+01	1.79E+01
3	1	PFC	Over-Expression	Random	1.54E+01	1.90E+01
3	2	PFC	Over-Expression	Random	2.17E+01	2.15E+01
7	1	HPC	Over-Expression	Overlapping	1.71E+01	1.79E+01
7	2	HPC	Over-Expression	Overlapping	2.22E+01	1.69E+01
9	1	PFC	Control	Random	1.63E+01	1.65E+01
9	2	PFC	Control	Random	2.18E+01	1.81E+01

Table 4.6: K-Means: intra-and inter-cluster Mahalanobis distances for rat one (HPC and control), three (PFC and over-expression), seven (HPC and over-expression) and nine (PFC and control)

4.4 FPP Clusters: Hidden Markov Model

The Hidden Markov Model had similar results to the K-Means clustering. The clusters looked like the former method; there was a compact CA1-hippocampal and less cohesive prelimbic prefrontal cortex clusters (figure 4.5). There was a separation across rats and regions of 20-80 and 80-120 Hz centred around 40 and 100 Hz, respectively, in the HPC.

The centres were around the ascending phase for the lower frequencies. The higher frequencies hovered around the peak and descending phase. The results from the PFC suggest a lower bound range of 20-80 with its core at approximately 40-60 and a higher bound of 80-120 centred around 100-110 Hz. The lower values varied on placement across the phase axis; they occurred at the ascending or descending phase differing per rat.

4.4.1 Significance: Intra-cluster & Inter-cluster

The Pearson distances found intra-and inter-cluster yielded similar to K-Means (table 4.7). Equivalently, the Mahalanobis distance also corroborates with the K-Means results by presenting smaller differences between inter-and intra-cluster than Pearson, yet having a more positive than negative outcome (table 4.8).

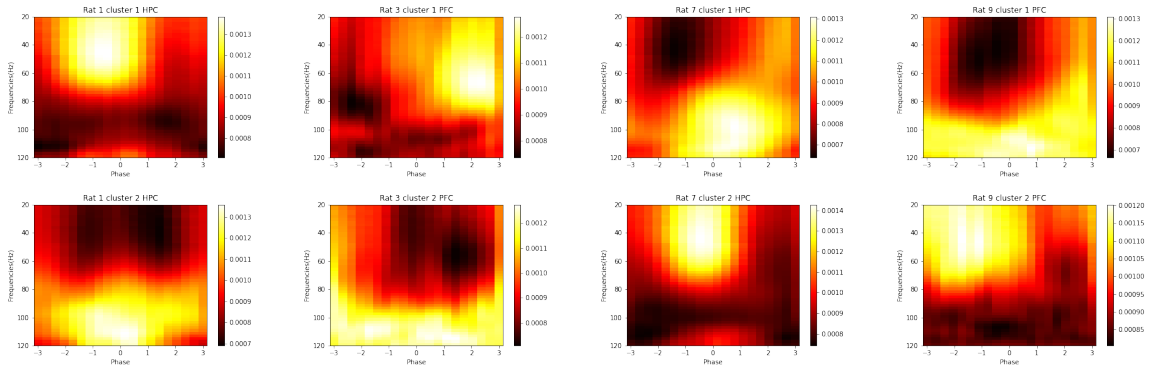

Figure 4.5: HMM of rat one (HPC, random and control), three (PFC, random and over-expression), seven (HPC, overlapping and over-expression) and nine (PFC, random and control)

Rat	Cluster Number	Region	Over-Expression/Control	Condition	Pearson Distance Inter	Pearson Distance Intra
1	1	HPC	Control	Random	6.32E-01	3.19E-01
1	2	HPC	Control	Random	6.20E-01	3.34E-01
3	1	PFC	Over-Expression	Overlapping	6.00E-01	3.62E-01
3	2	PFC	Over-Expression	Overlapping	6.11E-01	3.50E-01
7	1	HPC	Over-Expression	Overlapping	6.48E-01	3.39E-01
7	2	HPC	Over-Expression	Overlapping	6.21E-01	3.68E-01
9	1	PFC	Control	Random	6.46E-01	3.33E-01
9	2	PFC	Control	Random	6.05E-01	3.82E-01

Table 4.7: HMM: intra-and inter-cluster Pearson distances for rat one (HPC and control), three (PFC and over-expression), seven (HPC and over-expression) and nine (PFC and control)

Rat	Cluster Number	Region	Over-Expression/Control	Condition	Mahalanobis Distance Inter	Mahalanobis Distance Intra
1	1	HPC	Control	Random	1.75E+01	1.94E+01
1	2	HPC	Control	Random	1.77E+01	1.46E+01
3	1	PFC	Over-Expression	Overlapping	1.37E+01	1.69E+01
3	2	PFC	Over-Expression	Overlapping	1.93E+01	1.58E+01
7	1	HPC	Over-Expression	Overlapping	1.48E+01	1.61E+01
7	2	HPC	Over-Expression	Overlapping	1.68E+01	1.60E+01
9	1	PFC	Control	Random	2.20E+01	1.53E+01
9	2	PFC	Control	Random	1.99E+01	1.93E+01

Table 4.8: HMM: intra-and inter-cluster Mahalanobis distances for rat one (HPC and control), three (PFC and over-expression), seven (HPC and over-expression) and nine (PFC and control)

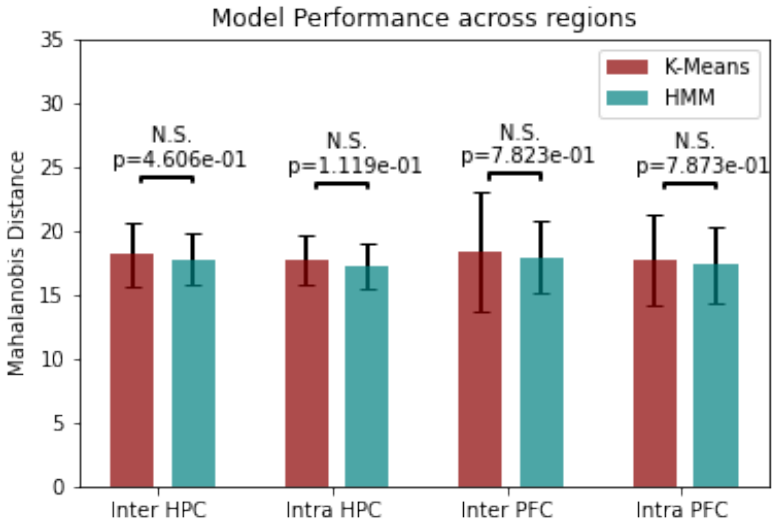

Figure 4.6: The averaged Mahalanobis results for the K-Means and HMM models for merged conditions. The Mann-Whitney p values signify the model differences, where N.S. is "Not Significant" and defined by p>0.05

4.5 Model Evaluation: Hidden Markov Model & K-Means

The HMM and K-Means models had similar results visually and statistically ($p > 5.00E-02$). This alignment increases the confidence in the results. Overall a visible decline is presented from inter-to intra-cluster distances, showing a generally positive outcome. Furthermore, it is notable that the standard deviation for the prelimbic prefrontal cortices is far more extended than that of the CA1 in the hippocampus, which is reflected in the cluster results (section 4.3.1 & 4.4.1). This standard deviation suggests more outliers within the PFC region. The model run time was approximately one minute for each condition, depending on the number of FPP vectors passed through. However, there was no distinct difference between the two models.

Chapter 5

Conclusion and Discussion

The main goal of this thesis was to assess and analyse correlation and clustering methods for finding distinguishable Theta-Gamma coupling in rats during REM sleep. Ultimately, I see a clear correlation between the used methods and measurements. From this distinction, I infer the correlation (Cross Frequency Coupling) and clustering methods, Community detection, K-Means, and HMM clustering, are adequate to analyse Theta-Gamma coupling.

The spectral analysis showed a high involvement of Theta and at least two relatively less involved Gamma sections around 40 and 100 Hz.

The correlational method examined the relationship between the frequencies, which resulted in an estimation of comodulation occurring for each rat per region, which aided in understanding the quality of clustering results. I found the random condition to have the best results, followed by home cage, stable and overlapping. The stable condition had very few REM sleep periods, so this condition's results are likely biased. Furthermore, there were some disparities between regions. There appeared to be a correlation between the general comodulation of the Theta and Gamma and the quality of comodulation in the hippocampus; if the hippocampal comodulation was lower than in the prelimbic prefrontal cortex, the overall condition's comodulation was also lower.

The clusters for rats per region were mostly aligned across our formerly found correlations and their different conditions, except for the stable state. The CA1-hippocampus clusters yielded relatively more clear segregation in the FPP matrices making more cohesive clusters than those in the prelimbic prefrontal cortex. These results were consistent across conditions and clustering methods. The model comparison showed the models' performance was similar. Predominately, a lower intra-cluster distance was found than inter, indicating a more compact internal bond as opposed to external. The Pearson distances corresponded with approximately 50% difference between the significance measurements with lesser intra-cluster results. The Mahalanobis distance did not yield equally strong results. However, this function aims to find outliers rather than inliers. The difference in approach might explain the bias within the results. Furthermore, Pearson assumes a linear relationship which may not be accurate, whereas Mahalanobis does not perhaps, yielding less prominent but more accurate results. Nonetheless, Mahalanobis distances

within all factors still yielded more favourable outcomes than not, showing our clusters are meaningful enough to pass through two distance measures with satisfying results.

The model evaluation displayed the proximity of both models; they nearly performed the same according to the distance functions. I noted high p values could be due to a lack of data. However, this is only known to consistently occur with less than seven data points. This sample issue is not the case in this thesis since there were 54 data points. So, it is reasonable to state that the models are similar. This result strengthens our thesis statement on K-Means and HMM in collaboration with Community Detection, being able to analyse Theta and Gamma interaction due to the alignment of results. Furthermore, generally positive results were discovered; inter-cluster distances were higher than intra-cluster for both models in the CA1-hippocampus and prelimbic prefrontal cortex. This proofs meaningful clusters are created with these methods. An extensive analysis would have to be performed to find small disparities between the two models.

In conclusion, this thesis established meaningful clusters by Community Detection, K-Means and Hidden Markov Models affirmed by a correlational Cross Frequency Coupling analysis. Evaluating the Theta-Gamma coupling through the methods in this thesis would give meaningful results. The clustering methods can divide the Gamma frequencies across the Theta phase and CFC analysis could help filter out poor data and reasoning on the clustering results.

5.1 Discussion

Multiple factors could be changed or expanded on in this thesis which made it hard to decide on the exact parameters and methods used. One of these factors is the number of clusters I utilised. The clustering algorithms relied on the Community Detection and our own bias for the best average number, the mean. This assumption could have heavily influenced the results.

Consequently, the fast Gamma was excluded from this thesis' clustering methods due to its vast range and overlap with other frequencies and noise. Pre-processing the fast Gamma in the data would have been a time-consuming task but worthwhile if all Gamma bands should be analysed. In this thesis, finding fast Gamma was not crucial and time did not allow it.

Another factor was the Distance measurements of the clusters; the neuroscientific nature of the data made it challenging to establish measurements for the success of the methods. The Mahalanobis distance measure was suggested by the thesis supervisors. This measure was not familiar which initially caused some confusion in the implementation and evaluation. Selecting the proper distance measures is dependent on the data, so this should be taken into consideration when using them to assess other methods' quality.

The last hurdle was time; the lack of optimisation and large datasets caused an increase in run time, especially the cross-frequency analysis and clustering intra- and extra-cluster calculations could take hours. The lack of time made it difficult to expand upon this thesis in this short period.

5.1.1 Future Work

Future work should focus on tackling the mentioned issues and the following factor; the clustering accuracy could be improved when all data is pulled together for over-expression and control rats. This merged data could increase the clustering accuracy and expand the coupling analysis but was hard to implement in this thesis since I had no established way of back-tracing the control/over-expression from the FPP matrices. Furthermore, it would be computationally heavy to experiment with this, making it infeasible in the given time frame.

In addition, performing an analysis on the proper clustering amount could be an independent thesis. These results could be implemented in a similar project to this thesis which would likely improve the clustering and analysis accuracy.

Another approach to explore is using a clustering method that does not require a cluster estimation. Therefore, the dependency is eliminated, allowing for a more independent approach. Furthermore, the run time for each model could be compared to the details for the two models. There were no noticeable run time differences without computational analysis. Lastly, many distance functions could be applied to measure the intra-and inter-cluster and perform the model evaluation, each having its respective benefits and limitations. Following studies should evaluate the distribution of the data and output of the functions.

I was able to discover substantial Theta-Gamma coupling with our methods. Countless factors could be adjusted other than the ones mentioned. However, the explained factors would likely increase the accuracy and further research should be able to implement expansions and improvements to analyse the relationship of frequencies more accurately. [nottoc,notlof,notlot]tocbibind

References

Amemiya, S. & Redish, A. D. (2018), 'Hippocampal theta-gamma coupling reflects state-dependent information processing in decision making', *Cell reports* **22**(12), 3328–3338.

Bueno-Junior, L. S. & Leite, J. P. (2018), 'Input convergence, synaptic plasticity and functional coupling across hippocampal-prefrontal-thalamic circuits', *Frontiers in Neural Circuits* **12**, 40.

Colgin, L., Denninger, T., Fyhn, M., Hafting, T., Bonnevie, T., Jensen, O., Moser, M. & Moser, E. (2009), 'Frequency of gamma oscillations routes flow of information in the hippocampus. nature [internet] 462: 353–357'.

Florian, B., Sepp, K., Joshua, H. & Richard, H. (2011), 'Hidden markov models in the neurosciences', *Hidden Markov Models, Theory and Applications* p. 169.

Genzel, L. (2020), 'Memory and sleep: brain networks, cell dynamics and global states', *Current Opinion in Behavioral Sciences* **32**, 72–79.

Genzel, L., Schut, E., Schröder, T., Eichler, R., Khamassi, M., Gomez, A., Navarro Lobato, I. & Battaglia, F. (2019), 'The object space task shows cumulative memory expression in both mice and rats', *PLoS biology* **17**(6), e3000322.

Genzel, L., Spoormaker, V., Konrad, B. & Dresler, M. (2015), 'The role of rapid eye movement sleep for amygdala-related memory processing', *Neurobiology of learning and memory* **122**, 110–121.

Genzel, L. & Wixted, J. T. (2017), Cellular and systems consolidation of declarative memory, *in* 'Cognitive neuroscience of memory consolidation', Springer, pp. 3–16.

Klinzing, J. G., Niethard, N. & Born, J. (2019), 'Mechanisms of systems memory consolidation during sleep', *Nature neuroscience* **22**(10), 1598–1610.

Koski, A. (1996), 'Modelling ecg signals with hidden markov models', *Artificial intelligence in medicine* **8**(5), 453–471.

Kramer, M. & Eden, U. (2020), 'Cross-frequency coupling', `https://mark-kramer.github.io/Case-Studies-Python/07.html#cross-frequency-coupling`.

Lasztóczi, B. & Klausberger, T. (2016), 'Hippocampal place cells couple to three different gamma oscillations during place field traversal', *Neuron* **91**(1), 34–40.

Martinez, E., Benadí, A., Toma, D., Delory, E., Gomariz, S. & del Rio, J. (2021), 'Metadata-driven universal real-time ocean sound measurement architecture', *IEEE Access* **PP**, 1–1.

Michelsen, K., Van den Hove, D., Schmitz, C., Segers, O., Prickaerts, J. & Steinbusch, H. (2007), 'Prenatal stress and subsequent exposure to chronic mild stress influence dendritic spine density and morphology in the rat medial prefrontal cortex', *BMC neuroscience* **8**, 107.

Poe, G. R., Nitz, D. A., McNaughton, B. L. & Barnes, C. A. (2000), 'Experience-dependent phase-reversal of hippocampal neuron firing during rem sleep', *Brain Research* **855**(1), 176–180.
URL: *https://www.sciencedirect.com/science/article/pii/S0006899399023100*

Samanta, A., Alonso, A. & Genzel, L. (2020), 'Memory reactivations and consolidation: considering neuromodulators across wake and sleep', *Current Opinion in Physiology* **15**, 120–127.

Schall, K. P. & Dickson, C. T. (2010), 'Changes in hippocampal excitatory synaptic transmission during cholinergically induced theta and slow oscillation states', *Hippocampus* **20**(2), 279–292.

Schomburg, E. W., Fernández-Ruiz, A., Mizuseki, K., Berényi, A., Anastassiou, C. A., Koch, C. & Buzsáki, G. (2014), 'Theta phase segregation of input-specific gamma patterns in entorhinal-hippocampal networks', *Neuron* **84**(2), 470–485.

Squire, L. R., Genzel, L., Wixted, J. T. & Morris, R. G. (2015), 'Memory consolidation', *Cold Spring Harbor perspectives in biology* **7**(8), a021766.

Szewczyk, B., PA, A., UCHA, M., GRUCA, P., MORYL, E. et al. (2001), 'Changes in the expression of metabotropic glutamate receptor 5 (mglur5) in the rat hippocampus in an animal model of depression', *Pol. J. Pharmacol* **53**, 659–662.

Welch, P. (1967), 'The use of fast fourier transform for the estimation of power spectra: a method based on time averaging over short, modified periodograms', *IEEE Transactions on audio and electroacoustics* **15**(2), 70–73.

Zhang, L., Lee, J., Rozell, C. & Singer, A. C. (2019), 'Sub-second dynamics of theta-gamma coupling in hippocampal ca1', *Elife* **8**, e44320.

Appendix A

Firwin filter

A.1 Coefficients

Algorithm 1 Pseudocode of the coefficient generation for the Firwin filtering

```
filter_band=filter_band/nyq
h= 0
for lower_band, upper_band in filter_band do
    x=make_periodic_array(lower_band)    ▷ array with length of coefficient amount
    y=make_periodic_array(upper_band)
    h += lower_higher * sine_cardinal(x)
    h -= upper_band * sine_cardinal(y)
end for
return Hamming_window(h)
```

A.2 Filtered Data: Sample

Figure A.1: Sample of REM sleep data in μV filtered into Theta, slow Gamma, medium Gamma and fast Gamma frequency bands

Appendix B

Cross Frequency Coupling: p value

The slow Gamma's true value overlaps with its surrogates in both images, whereas the medium Gamma only slightly overlaps in the left and not in the right image.

Figure B.1: Random sample of random epochs excluding Fast Gamma

Appendix C

HMM Theoretical Problems

C.1 Evaluation Problem

The v's are the observed non-clustered FPP vector states ω's are the hidden FPP clusters, T is the finite time, the Theta cycle length in radians from $-pi$ to pi, and R is the number of hidden states, Gamma clusters in the Theta phase.

$$\begin{aligned} R = \{\omega_r, \omega_{r+1}, \ldots, \omega_R\}, \omega_r^T = \{\omega(1), \omega(2), \ldots, \omega(T)\} \\ P(\omega_r^T) = \prod_{t=1}^{T} P(\omega(t)|\omega(t-1)) \\ P(v^T|\omega_r^T) = \prod_{t=1}^{T} P(v(t)|\omega(t)) \\ P(v^T|\theta) = \sum_{r=1}^{R} P(v^T|\omega_r^T)P(\omega_r^T) = \sum_{r=1}^{R}\prod_{t=1}^{T} P(v(t)|\omega(t)P(\omega(t)|\omega(t-1)) \end{aligned} \tag{C.1}$$

C.2 Learning Problem

The Θ are the model parameters, η is the step size and L_{total} is the sum of transition and emission probabilities for a state t. The a and b are the transition and emission probabilities, respectively.

$$\begin{aligned} \Theta^{New} = \Theta^{Old} - \eta[\frac{\delta J}{\delta \Theta}]_{\Theta=\Theta^{Old}} \\ \frac{\delta J}{\delta \Theta} = -\frac{1}{L_{total}}\frac{\delta L_{total}}{\delta \Theta} \\ L_{total} = \sum_i a(i)b(i) \end{aligned} \tag{C.2}$$

C.3 Decoding Problem

The θ is the instantiated model, q_t is the most likely state, v is the actual visible state and j^* is one of the states in the sequence of hidden states.The i is the current state and t is a time sequence for 1<t<T-1. The α_{t+1} is the forward variable of the state and $\delta_t + 1$ is the likelihood of the next state. The transition probability is $a_i j$ for the current, i, and most likely state, j. Lastly, the emission state, b_j is the emission of the most likely state.

$$\begin{aligned} \delta_t(i) &= \max_q [p(q_t = v|\theta)] \\ \delta_{t+1}(j) &= b_j(\alpha_{t+1}) \max_{1<i<N} [\delta_t(i) * a_{ij}] \\ j^* &= arg \max_{1<j<N} [\delta_T(j)] \end{aligned} \tag{C.3}$$

Appendix D

Significance and Distance measurements

D.1 The p value

In this function *cdf* is the cumulative density function and st is the statistic measured.

$$p = 1 - cdf(st) \tag{D.1}$$

D.2 Intra-cluster Distance

In this function c_i is a single FPP vector (1×1020) and c_k is the mean of all vectors in the same cluster, giving a 1D vector. The d is described by a specific distance function.

$$\begin{matrix} d(c_i, c_k) \\ \Big\{ c_i, c_k \in S_i \end{matrix} \tag{D.2}$$

D.3 Inter-cluster Distance

In this function, c_i is a single FPP vector (1×1020) and c_j is the mean of all vectors in a cluster outside the former's cluster. M is the number of clusters instantiated by Community Detection minus one. The d is described by a specific distance function.

$$\begin{matrix} \frac{1}{M} \sum_{j}^{M} d(c_i, c_j) \\ \begin{cases} c_i \in S_i \\ c_j \in S_j \text{ for all } j \\ S_i \notin \{S_j, .., S_M\} \end{cases} \end{matrix} \tag{D.3}$$

-

D.4 Pearson Coefficient and Distance

The x_n and y_n are points in the FPP vectors. The $\bar{x}$ and $\bar{y}$ are the means of the vectors. N is the number of points in the FPP data.

$$r = \frac{\sum_{n=1}^{N}(x_n - \bar{x})(y_n - \bar{y})}{\sqrt{\sum_{n=1}^{N}(x_n - \bar{x})^2 \sum_{n}^{N}(y_n - \bar{y}^2)}} \qquad d(x,y) = (1-r)/2 \tag{D.4}$$

D.5 Mahalanobis Distance

Cov takes the covariance matrix of the FPP vectors. To reiterate, The x_n and y_n are points in the FPP vectors. The $\bar{x}$ and $\bar{y}$ are the means of the vectors. N is the number of points in the FPP data.

$$d(x,y) = \frac{1}{N}\sum_{n}^{N}\sqrt{(x_n - y_n)V^{-1}(x_n - y_n)^T} \qquad V^{-1} = Cov(x,y)^{-1} \qquad Cov(x,y) = \sum_{n}^{N}(x_n - \bar{x})(y_n - \bar{y}) \tag{D.5}$$